Applied Catalysis B: Environmental 90 (2009) 184–194

Contents lists available at ScienceDirect

Applied Catalysis B: Environmental

journal homepage: www.elsevier.com/locate/apcatb

Factors influencing the electrocatalytic activity of $Pd_{100-x}Co_x$ ($0 \leq x \leq 50$) nanoalloys for oxygen reduction reaction in fuel cells

H. Liu, W. Li, A. Manthiram *

Electrochemical Energy Laboratory & Materials Science and Engineering Program, The University of Texas at Austin, Austin, TX 78712, United States

ARTICLE INFO

Article history:
Received 14 August 2008
Received in revised form 14 February 2009
Accepted 3 March 2009
Available online 17 March 2009

Keywords:
Fuel cells
Electrocatalyst
Palladium alloys
Oxygen reduction reaction

The factors that control the electrocatalytic activity for the oxygen reduction reaction (ORR) in fuel cells have been investigated systematically with the low cost carbon-supported $Pd_{100-x}Co_x$ ($0 \leq x \leq 50$) nanoalloys. The $Pd_{100-x}Co_x$/C samples have been prepared by a solution-based reduction procedure and annealed at 350 and 500 °C. While the catalytic activity of the as-prepared samples decreases monotonously with nominal Co content due to poor alloying and instability, a volcano type dependence of the activity on Co content with the maximum at around a nominal Co content of 25 at% Co or an actual Co content of about 10 at% in the Pd lattice (degree of alloying) is found for the samples annealed at 350 and 500 °C due to the influence of both the degree of alloying and variations in crystallite size. Below 30 at% nominal Co content, the catalytic activity of the annealed samples increases with increasing nominal Co content due to both a decreasing crystallite size and increasing degree of alloying. For 30–50 at% nominal Co content, the catalytic activity decreases with Co content due to increasing degree of alloying as the crystallite size remains constant. The durability of the catalyst increases with annealing due to both an increase in the degree of alloying and crystallite size.

1. Introduction

Platinum supported on carbon remains to be the state-of-the art electrocatalyst for the oxygen reduction reaction (ORR) both in proton exchange membrane fuel cells (PEMFC) and direct methanol fuel cells (DMFC) due to its high catalytic activity and stability [1–3]. However, the high cost and limited natural abundance of platinum pose serious challenges for the commercialization of the PEMFC and DMFC technologies. In this regard, several less expensive electrocatalysts such as carbides [4], oxides [5], enzymes [6,7], and platinum-free alloys [8–10] as well as alloying of Pt with other non-noble metals like Co, Fe, Ni [11–14], and reduction in the catalyst loading [15–20] have been widely investigated over the years for ORR. Recently, we showed that palladium-based alloy catalysts such as Pd–Co–Mo, Pd–Co–Au, Pd–Co and Pd–Ti exhibit high electrocatalytic activity for ORR [21–24] with a significant reduction in cost compared to Pt; the cost of Pd is one-fifth of the cost of Pt. Data from other groups [10,25–28] have also shown that alloying Pd with other elements such as Cr, Co, Fe, Ni, Ru, and Au increase the catalytic activity of Pd for ORR. Theoretical studies have suggested that the enhanced catalytic activity on alloying Pd with other elements like Fe, Co, and Ni originates from the optimum surface electronic structure in the presence of other alloying elements [29,30].

Among them, the Pd–Co alloys are particularly interesting as they offer high electrocatalytic activity for ORR along with high tolerance to methanol that may crossover from the anode to the cathode. However, compared to the extensive studies on the enhanced catalytic activity of Pt–Co alloys for ORR [11–13], relatively less information is available on the Pd–Co electrocatalysts. Also, both the catalytic activity and durability can be sensitively influenced by particle size, particle shape, compositional homogeneity, and surface structure [31]. For example, the specific activity of Pt has been reported to decrease with decreasing crystallite size below 6 nm [32,33]. More interestingly, a recent report has shown that Pt crystals with high-index facets and a crystallite size of >50 nm exhibit 4-fold enhancement in catalytic activity compared to the commercial Pt catalyst having similar surface area and a particle size of 3 nm [3]. However, little is known on the effect of crystallite size, composition, degree of alloying, and surface structure of Pd–Co alloys on their catalytic activity and durability. Moreover, the actual degree of alloying (incorporation of Co into the Pd crystal lattice) could often be different from the nominal composition depending on the synthesis conditions and the post annealing temperatures. While the annealing generally helps to increase the degree of alloying, it also leads to a growth in crystallite size and a consequent decrease in surface area and catalytic activity.

* Corresponding author. Tel.: +1 512 4711791; fax: +1 512 4717681.
E-mail address: rmanth@mail.utexas.edu (A. Manthiram).

0926-3373/$ – see front matter © 2009 Elsevier B.V. All rights reserved.
doi:10.1016/j.apcatb.2009.03.008

These opposing effects lead to difficulties in precisely understanding the roles of the various factors on the catalytic activity and durability of Pd–Co alloy catalysts and understanding the catalytic mechanisms involved.

To address these challenging issues, we present here a systematic investigation of carbon-supported Pd–Co electrocatalysts with various Co contents that are synthesized by a modified polyol reduction process followed by annealing at various temperatures and characterized. The effects of Co content, degree of alloying, and crystallite size on the electrocatalytic activity for ORR are discussed.

2. Experimental

Carbon-supported $Pd_{100-x}Co_x$ ($0 \le x \le 50$) electrocatalysts with a metal(s) loading of 20 wt.% were prepared by a modified polyol reduction process described below. Required amounts of $(NH_4)_2PdCl_4$ (Aldrich) and $CoCl_2{\cdot}6H_2O$ (Alfa Aesar) to obtain 100 mg of $Pd_{100-x}Co_x$/C were dissolved in 40 mL of a mixed solution containing ethylene glycol (EG, a polyol) and water in the volume ratio of 2:1 by magnetic stirring. 25 mg of poly(vinylpyrrolidone) (PVP, MW = 40,000) was then dissolved in the above solution by magnetic stirring. After vigorous stirring for 1 h, a freshly prepared solution of $NaBH_4$ (Alfa Aesar) containing 200 mg of $NaBH_4$ in 40 mL of water was added dropwise under stirring, the mixture was refluxed at 130 °C for 2 h under a flowing nitrogen atmosphere, and cooled to room temperature. To the dark brown or black colloidal solution thus formed, an appropriate amount of carbon (Vulcan XC 72R) was added to give a metal(s):C weight ratio of 20:80 and kept under constant stirring for 2 h. The slurry was filtered, washed copiously with ethanol and deionized water, and dried in an oven overnight at 100 °C. The as-prepared powders thus obtained are denoted hereafter as $Pd_{100-x}Co_x$/C-Ap. Examination of the as-prepared samples by a Perkin Elmer FT-IR System (Spectrum BX) indicated that no residual PVP is present. The as-prepared samples were then annealed at 350 and 500 °C in a flowing mixture of 10% H_2–90% Ar for 2 h and cooled to room temperature with a cooling rate of 5 °C min^{-1}, which are hereafter denoted, respectively, as $Pd_{100-x}Co_x$/C-350 and $Pd_{100-x}Co_x$/C-500.

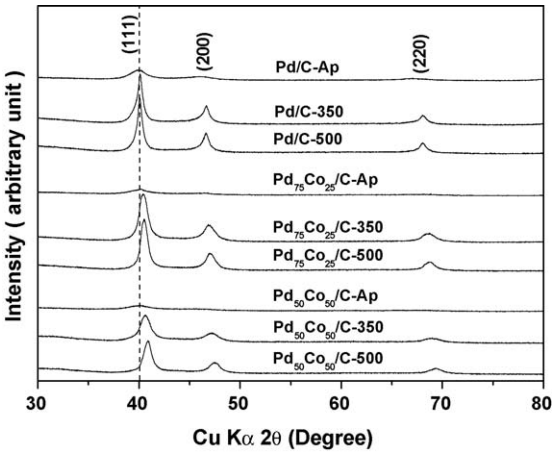

Fig. 1. XRD patterns of the Pd/C, $Pd_{75}Co_{25}$/C and $Pd_{50}Co_{50}$/C electrocatalysts before and after annealing in 10% H_2–90% Ar atmosphere at various temperatures. The dashed vertical line indicates the standard 2θ value corresponding to the (1 1 1) reflection of Pd metal.

All the samples were characterized by X-ray diffraction (XRD) using Cu Kα radiation. The average crystallite sizes were assessed by analyzing the XRD data with the Jade 7.0 program employing Scherrer equation. The electrochemical characterization was carried out by cyclic voltammetry (CV) using a glassy carbon (GC) micro-electrode in a classical three-electrode system with 0.5 M H_2SO_4 electrolyte solution at room temperature. In the three-electrode test cell, the GC micro-electrode was taken as the working electrode and a Pt net and a saturated calomel electrode (SCE) were used, respectively, as the counter and reference electrodes. The GC micro-electrode was prepared as described below. 5 mg of the carbon-supported electrocatalyst synthesized was mixed with 1 mL of ethanol and ultrasonicated for 25 min to form an ink. 5 μL of the ink was then cast onto the GC electrode surface to form a thin film of electrocatalyst, followed by the application of 2 μL of 5% Nafion solution (Du Pont) to the thin film surface and drying the coating at 100 °C. The CV curves were obtained by multi-cycle scans with a sweep rate of 20 mV s^{-1} in the potential window of −0.24

Table 1
Characterization data of the $Pd_{100-x}Co_x$/C electrocatalysts.

Samples	Lattice parameter from XRD (nm)	Average crystallite size from XRD[a] (nm)	Degree of alloying: atomic percent Co in the sample (%)	Surface area S_A ($m^2\ g^{-1}$)
$Pd_{50}Co_{50}$/C-Ap	–	3.1 (1)	0	207.4
$Pd_{50}Co_{50}$/C-350	3.8508 (6)	5.5 (1)	15.0	113.5
$Pd_{50}Co_{50}$/C-500	3.8253 (2)	6.7 (2)	24.7	91.3
$Pd_{60}Co_{40}$/C-Ap	–	3.3 (1)	0	184.3
$Pd_{60}Co_{40}$/C-350	3.8530 (8)	5.6 (1)	14.1	107.5
$Pd_{60}Co_{40}$/C-500	3.8327 (2)	7.2 (1)	21.9	80.8
$Pd_{70}Co_{30}$/C-Ap	–	3.7 (2)	0	156.0
$Pd_{70}Co_{30}$/C-350	3.8632 (9)	5.8 (1)	10.2	97.5
$Pd_{70}Co_{30}$/C-500	3.8394 (9)	7.5 (2)	19.3	74.1
$Pd_{75}Co_{25}$/C-Ap	–	3.8 (1)	0	148.0
$Pd_{75}Co_{25}$/C-350	3.8728 (8)	7.0(1)	6.5	79.3
$Pd_{75}Co_{25}$/C-500	3.8619 (7)	9.1 (2)	10.7	60.5
$Pd_{80}Co_{20}$/C-Ap	–	3.6 (1)	0	152.4
$Pd_{80}Co_{20}$/C-350	3.8768 (8)	8.1 (1)	4.9	67.1
$Pd_{80}Co_{20}$/C-500	3.8692 (7)	10.2 (2)	7.90	52.9
$Pd_{90}Co_{10}$/C-Ap	–	3.9 (1)	0	134.1
$Pd_{90}Co_{10}$/C-350	3.8848 (8)	10.6 (2)	1.84	49.2
$Pd_{90}Co_{10}$/C-500	3.8814 (3)	12.8 (2)	3.22	40.6
$Pd_{100}Co_0$/C-Ap (Pd/C-Ap)	3.8895 (2)	4.0 (2)	0	125.0
$Pd_{100}Co_0$/C-350 (Pd/C-350)	3.8894 (3)	8.7 (2)	0	57.5
$Pd_{100}Co_0$/C-500 (Pd/C-500)	3.8895 (2)	10.8 (2)	0	46.3

[a] Obtained using (2 2 0) reflections.

to 1.1 V vs. SCE and the electrochemical active surface area and durability of the $Pd_{100-x}Co_x$/C samples was obtained from the surface oxide reduction peak area. Nitrogen gas was bubbled through the electrolyte solution to keep a clean reaction atmosphere.

The CV data were complemented by evaluating the electrocatalytic activity for ORR by the single cell PEMFC measurements and linear polarization (LP) measurements using a rotating disk electrode (RDE). For the single cell PEMFC measurements, the electrodes consisted of gas-diffusion and catalyst layers. The anode catalyst was a commercial 20 wt.% Pt/C (E-TEK) and the cathode catalysts were the synthesized $Pd_{100-x}Co_x$ samples. The electrodes were impregnated with Nafion solution (5 wt.% solution, DuPont Fluoro-products) by a spray technique and dried at 90 °C under vacuum for 30 min. The loadings for both the anode and cathode were 0.4 mg cm^{-2}, and the Nafion loading for both the anode and cathode catalysts were 0.5 mg cm^{-2}. The membrane–electrode assemblies (MEAs) were fabricated by uniaxially hot-pressing the anode and cathode onto a Nafion 112 membrane (DuPont) at 140 °C for 2 min. The electrochemical performances in PEMFC of the MEAs were evaluated with a single-cell fixture having an active area of 5 cm^2 and feeding humidified H_2 into the anode at a flow rate of 100 mL min^{-1} with a back pressure of 14 psi and humidified oxygen into the cathode at a flow rate of 200 mL min^{-1} with a back pressure of 15 psi. The temperatures of humidified H_2 and oxygen were same as that of the cell temperature (60 °C). The LP-RDE measurements were carried out with the same three-electrode system used for the CV tests with 0.5 M H_2SO_4 electrolyte solution saturated with oxygen at a scan potential from 1.0 to 0.1 V vs. NHE with a sweep rate of 5 mV s^{-1}. A 5 mm diameter glassy carbon rotating disk micro-electrode was taken as the working electrode and the micro-electrode was prepared by the same procedure described for the CV tests. The rotating rate was fixed at 1600 rpm. All the electrode potential values attained in the LP tests were treated with *iR* correction.

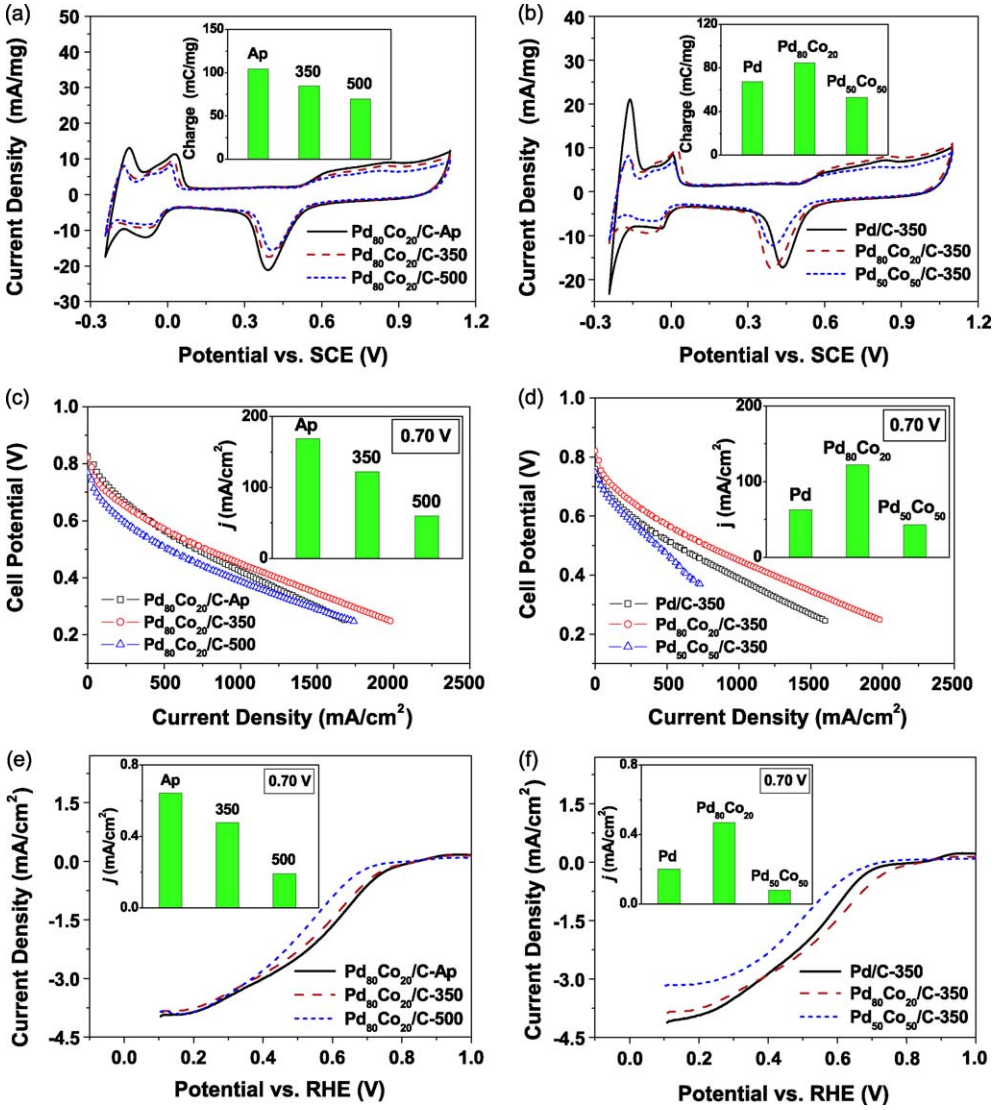

Fig. 2. Comparison of the catalytic activities for ORR of the $Pd_{80}Co_{20}$/C samples before and after annealing at various temperatures and the Pd/C, $Pd_{80}Co_{20}$/C, and $Pd_{50}Co_{50}$/C samples after annealing at 350 °C: (a) 15th cycle CV curves of $Pd_{80}Co_{20}$/C-Ap, $Pd_{80}Co_{20}$/C-350 and $Pd_{80}Co_{20}$/C-500, (b) 15th cycle CV curves of Pd/C-350, $Pd_{80}Co_{20}$/C-350, and $Pd_{50}Co_{50}$/C-350, (c) polarization curves recorded in single cell PEMFC of $Pd_{80}Co_{20}$/C-Ap, $Pd_{80}Co_{20}$/C-350, and $Pd_{80}Co_{20}$/C-500, (d) polarization curves recorded in single cell PEMFC of Pd/C-350, $Pd_{80}Co_{20}$/C-350, and $Pd_{50}Co_{50}$/C-350, (e) linear polarization curves recorded in RDE of $Pd_{80}Co_{20}$/C-Ap, $Pd_{80}Co_{20}$/C-350 and $Pd_{80}Co_{20}$/C-500, and (f) linear polarization curves recorded in RDE of Pd/C-350, $Pd_{80}Co_{20}$/C-350, and $Pd_{50}Co_{50}$/C-350. The insets compare the catalytic activity using the 15th cycle surface oxide reduction peak area in (a) and (b) and the catalytic activity by comparing the current density at 0.70 V in (c)–(f).

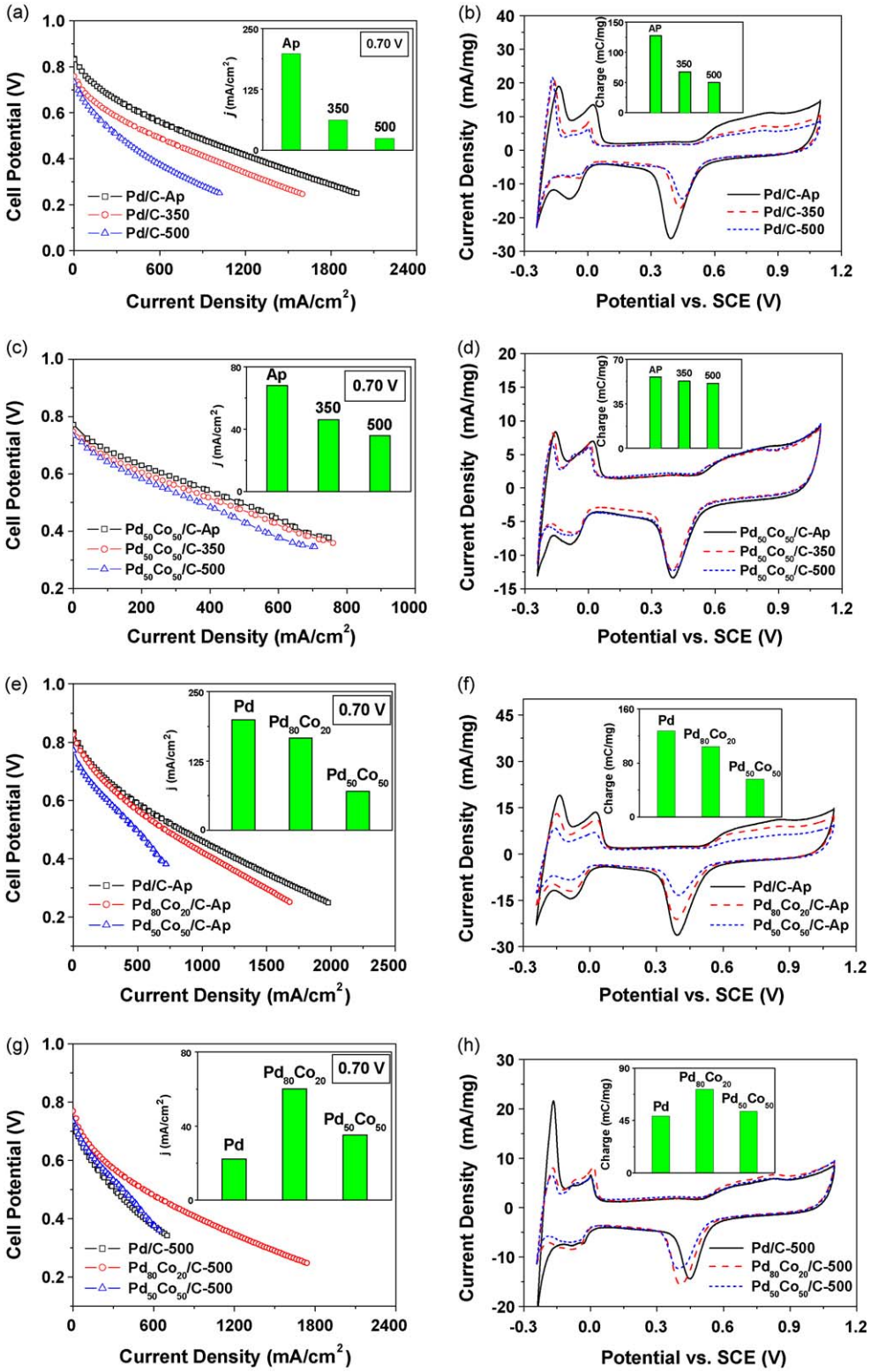

Fig. 3. Comparison of the catalytic activities for ORR of the Pd/C, $Pd_{50}Co_{50}$/C samples before and after annealing at various temperatures and the Pd/C, $Pd_{80}Co_{20}$/C, and $Pd_{50}Co_{50}$/C samples before and after annealing at 500 °C: (a) polarization curves recorded in single cell PEMFC of Pd/C-Ap, Pd/C-350, and Pd/C-500, (b) 15th cycle CV curves of Pd/C, Pd/C-350 and Pd/C-500, (c) polarization curves recorded in single cell PEMFC of $Pd_{50}Co_{50}$/C-Ap, $Pd_{50}Co_{50}$/C-350, and $Pd_{50}Co_{50}$/C-500, (d) 15th cycle CV curves of $Pd_{50}Co_{50}$/C-Ap, $Pd_{50}Co_{50}$/C-350, and $Pd_{50}Co_{50}$/C-500, (e) polarization curves recorded in single cell PEMFC of Pd/C-Ap, $Pd_{80}Co_{20}$/C-Ap, and $Pd_{50}Co_{50}$/C-Ap, (f) 15th cycle CV curves of Pd/C-Ap, $Pd_{80}Co_{20}$/C-Ap, and $Pd_{50}Co_{50}$/C-Ap, (g) polarization curves recorded in single cell PEMFC of Pd/C-500, $Pd_{80}Co_{20}$/C-500, and $Pd_{50}Co_{50}$/C-500, and (h) 15th cycle CV curves of Pd/C-500, $Pd_{80}Co_{20}$/C-500, and $Pd_{50}Co_{50}$/C-500. The insets compare the catalytic activity by comparing the current density at 0.70 V in (a), (c), (e) and (g), and the 15th cycle surface oxide reduction peak area in (b), (d), (f) and (h).

3. Results and discussion

Fig. 1 compares the XRD patterns of the $Pd_{100-x}Co_x/C$ samples with different Co contents before and after annealing at various temperatures in the reducing atmosphere. The data indicate the formation of single phase materials with a face-centered cubic structure. The reflections of $Pd_{75}Co_{25}/C$ and $Pd_{50}Co_{50}/C$ are shifted to higher angles compared to those of Pd/C (indicated by a dash line in Fig. 1) after annealing at 350 and 500 °C, confirming the substitution of smaller Co atoms for the larger Pd atoms (degree of alloying) in the Pd lattice. The movement of the reflections to higher angles on going from the as-prepared to the 350 and 500 °C annealed samples also suggests an increase in the degree of alloying on annealing. The lattice parameter values, degree of alloying (at% Co incorporated into the Pd lattice) [28], and crystallite size values obtained from the XRD data using the Scherrer equation are shown in Table 1. The degree of alloying, denoted as the *x* at% Co in the Pd lattice, was estimated from the lattice parameter values obtained from the XRD data using the empirical equation,

$$x\left(1-\frac{r_{Co}}{r_{Pd}}\right)=1-\frac{a_{alloy}}{a_{Pd}} \quad (1)$$

where *r* is the metallic radius of Pd or Co and a_{Pd} and a_{alloy} are, respectively, the lattice parameter values of Pd and Pd–Co alloy. The lattice parameter values of the as-prepared Pd–Co/C samples (excepting Pd/C-Ap) could not be obtained as the reflections were too broad. Also, since no clear shifts in the positions of reflections of the as-prepared Pd–Co/C samples compared to those of Pd/C are seen, the degree of alloying (at% Co in the Pd lattice) is considered to be zero. However, the degree of alloying and the crystallite size increase with increasing annealing temperature for the Pd–Co/C samples as seen in Table 1.

Fig. 2 provides a comparison of the catalytic activities for ORR of the $Pd_{80}Co_{20}/C$ samples before and after annealing at 350 and 500 °C and that of the Pd/C, $Pd_{80}Co_{20}/C$ and $Pd_{50}Co_{50}/C$ samples after annealing at 350 °C. Fig. 2(a and b) compares the CV scans recorded at the 15th cycle for the samples. Since the electrochemical surface area of the studied catalysts can be proportional to the cathodic peak area of the surface oxide reduction region [28] in Fig. 2(a and b) and all the micro-electrodes for the CV tests contained the same mass of the samples, the specific mass cathodic peak area values normalized to the sweep rate (*i.e.* charge transferred or cathodic peak area divided by the sweep rate) is used in this study to compare the relative electrocatalytic activity for ORR of the different samples. The insets in Fig. 2(a and b) compare the relative catalytic activity at the 15th cycle. To confirm the trend observed with the CV data, the catalytic activity for ORR was also evaluated with single cell PEMFC measurements as well as linear polarization measurements using RDE in 0.5 M H_2SO_4 electrolyte solution saturated with oxygen employing the same three-electrode system used for the CV test. Fig. 2(c and d) compares the polarization curves recorded with single cell PEMFC. The comparison of the current density values at 0.70 V, which is in the activation overpotential controlled region of ORR, is shown in the insets of Fig. 2(c and d). Fig. 2(e and f) displays the linear polarization curves recorded with RDE and the insets compare the electrochemical activity obtained by extracting the current density values from the LP-RDE curves at 0.70 V. A comparison of the data in the insets of Fig. 2(a–f) reveals that the trends found in the CV data are consistent with the trends found with the PEMFC and LP-RDE data.

For further confirming the trends of the relative catalytic activities revealed by CV, a comparison of the single cell PEMFC and 15th cycle CV data of the Pd/C and $Pd_{50}Co_{50}/C$ samples before and after annealing at 350 and 500 °C is provided in Fig. 3(a–d). Also, a similar comparison of the Pd/C, $Pd_{80}Co_{20}/C$ and $Pd_{50}Co_{50}/C$ samples before and after annealing at 500 °C is shown in Fig. 3(e–h). The insets in the PEMFC plots compare the trends of the current density values at 0.70 V, *i.e.* at the activation overpotential controlled region of ORR. The insets in the CV plots compare the relative catalytic activities obtained from the peak area of the 15th cycle. A comparison of the data in the insets of

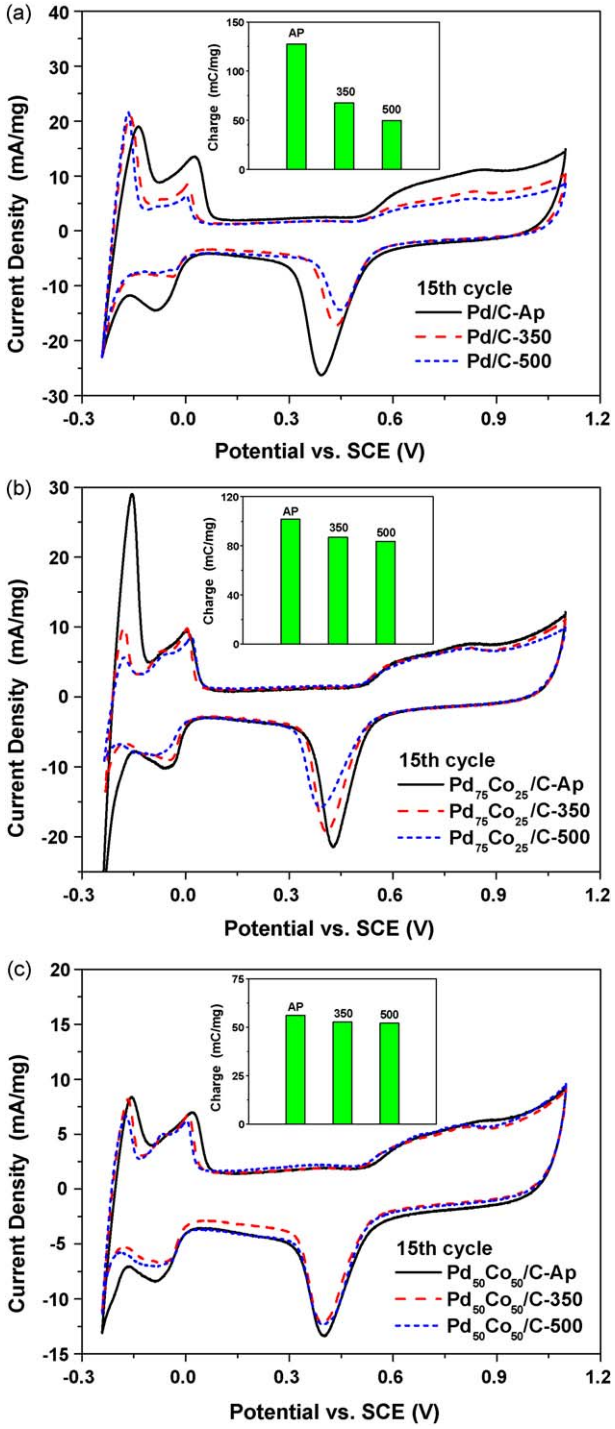

Fig. 4. The CV scans of the Pd/C, $Pd_{75}Co_{25}/C$ and $Pd_{50}Co_{50}/C$ samples (after annealing at various temperatures) recorded at the 15th cycle in 0.5 M H_2SO_4 solution at a sweep rate of 20 mV s^{-1} at room temperature: (a) Pd/C, (b) $Pd_{75}Co_{25}/C$-350, and (c) $Pd_{50}Co_{50}/C$. The insets in each figure compare the 15th cycle mass activity (or surface oxide reduction peak area).

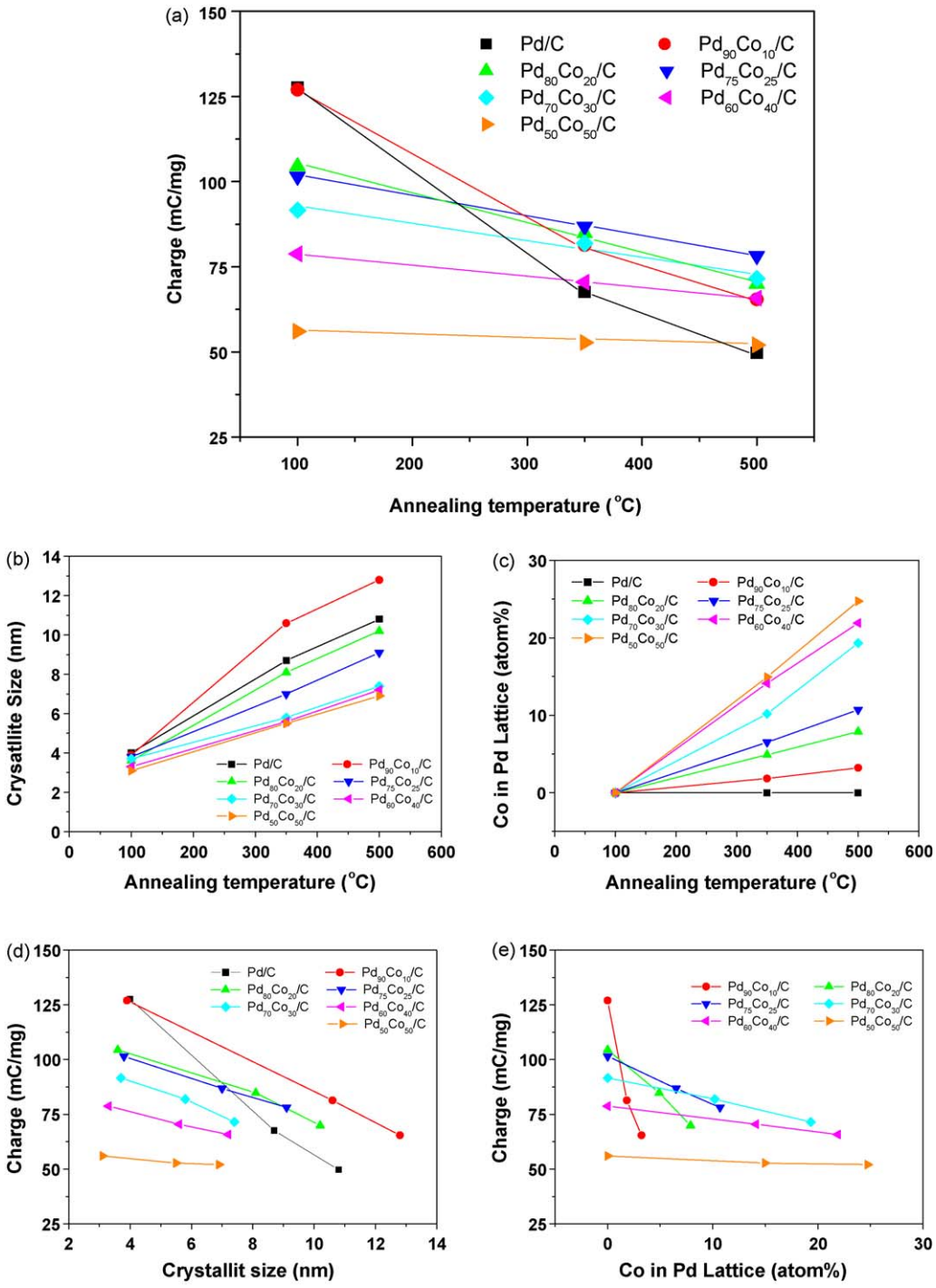

Fig. 5. Variations of (a) catalytic activity with annealing temperature, (b) crystallite size with annealing temperature, (c) degree of alloying (Co content in the Pd lattice) with annealing temperature, (d) catalytic activity with crystallite size, and (e) catalytic activity with degree of alloying for the $Pd_{100-x}Co_x/C$ electrocatalysts.

Fig. 3(a–h) reveals that the trends of the CV data are highly consistent with the trends of the PEMFC data, suggesting that the surface oxide reduction peak area in the CV plots could be used to assess the relative catalytic activities of different samples.

Fig. 4 compares the CV scans recorded at the 15th cycle in 0.5 M H_2SO_4 electrolyte at room temperature of Pd/C, $Pd_{75}Co_{25}/C$, and $Pd_{50}Co_{50}/C$ before and after annealing at various temperatures. The insets in Fig. 4 compare the surface oxide reduction peak area at the 15th cycle. Although the onset potential does not vary significantly, the peak area or electrocatalytic activity decreases with annealing temperature for all the three samples. However, the decrease in activity with annealing temperature diminishes as the Co content in Pd–Co increases. This could be attributed to the effects of increasing degree of alloying and crystallite size with annealing temperature.

Fig. 5(a) shows the variations of the catalytic activity with annealing temperature for the $Pd_{100-x}Co_x/C$ samples with various Co contents. The catalytic activity generally decreases with increasing annealing temperature although the decrease becomes less pronounced with increasing nominal Co content. However, both the crystallite size and the degree of alloying (Co content in the Pd lattice) increase with annealing temperature as seen in

Fig. 5(b and c) although the increase in crystallite size becomes less pronounced and the increase in degree of alloying becomes more pronounced with increasing nominal Co content. Clearly, the crystallite growth is suppressed by increasing nominal Co content. Fig. 5(d and e) shows the variations of catalytic activity with crystallite size and Co content in the Pd lattice. While the decrease in the catalytic activity of Pd/C with annealing temperature can be considered exclusively to be due to the increase in crystallite size, those of the Pd–Co/C samples could be influenced both by the increase in crystallite size and the degree of alloying.

Table 1 gives the particle surface area S_A in $m^2\,g^{-1}$ that is calculated using the equation $S = 6000/r\rho$ for spherical particles [23], where r is the crystallite size (diameter) in nm obtained from the XRD data and ρ is the density of the Pd–Co samples in

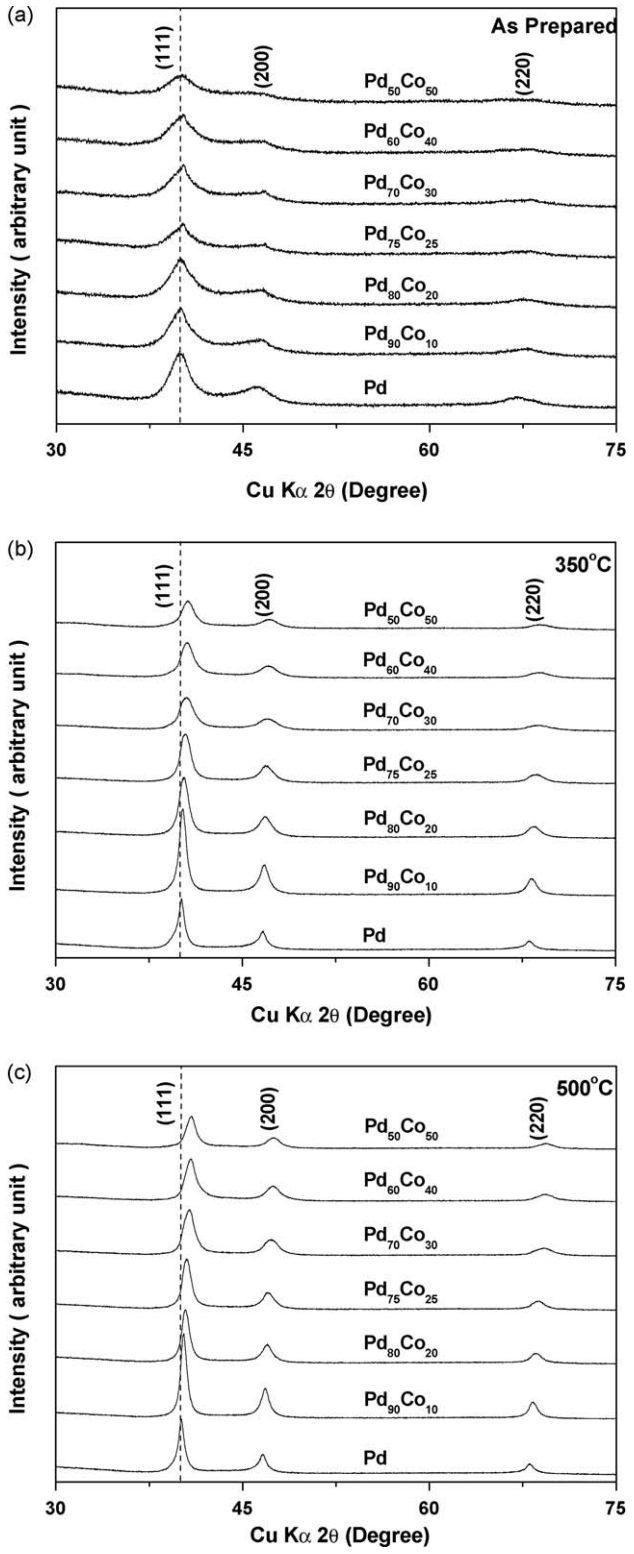

Fig. 6. XRD patterns of the $Pd_{100-x}Co_x/C$ electrocatalysts with various nominal Co contents: (a) as-prepared samples, (b) after annealing at 350 °C, and (c) after annealing at 500 °C. The dashed vertical line indicates the standard 2θ value corresponding to the (1 1 1) reflection of Pd metal.

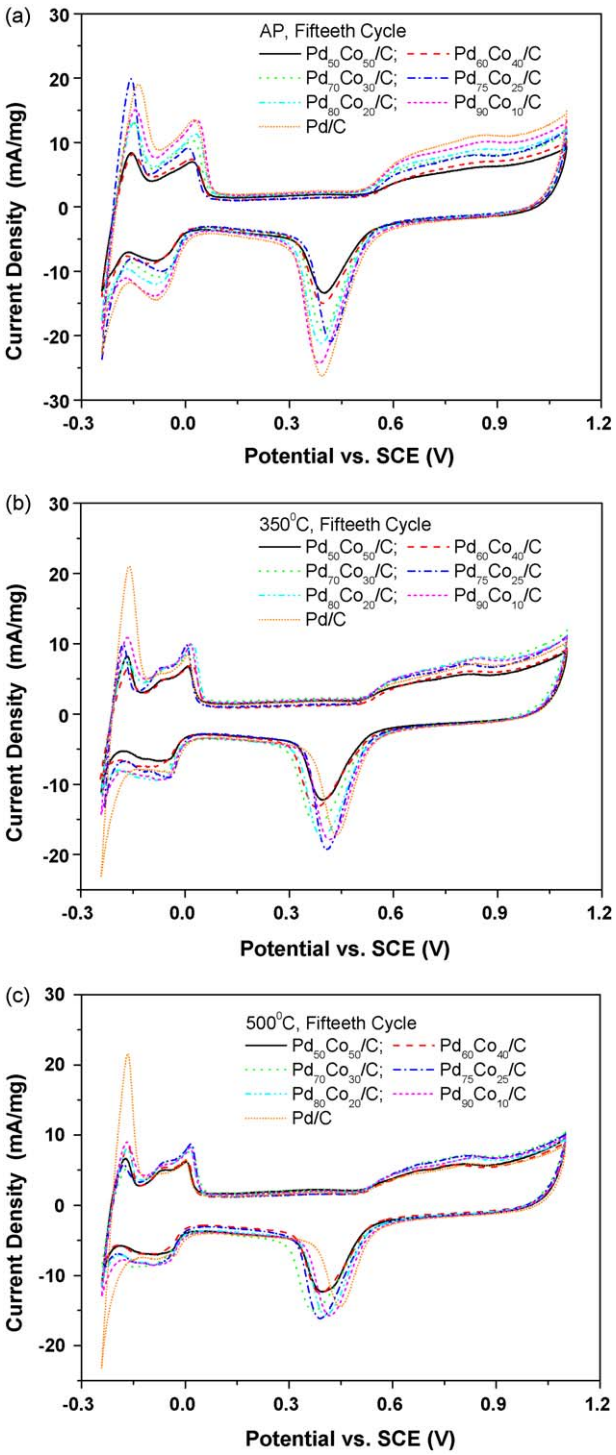

Fig. 7. CV scans of the $Pd_{100-x}Co_x/C$ electrocatalysts recorded at the 15th cycle in 0.5 M H_2SO_4 electrolyte at a sweep rate of 20 mV s^{-1} at room temperature: (a) as-prepared samples, (b) after annealing at 350 °C, and (c) after annealing at 500 °C.

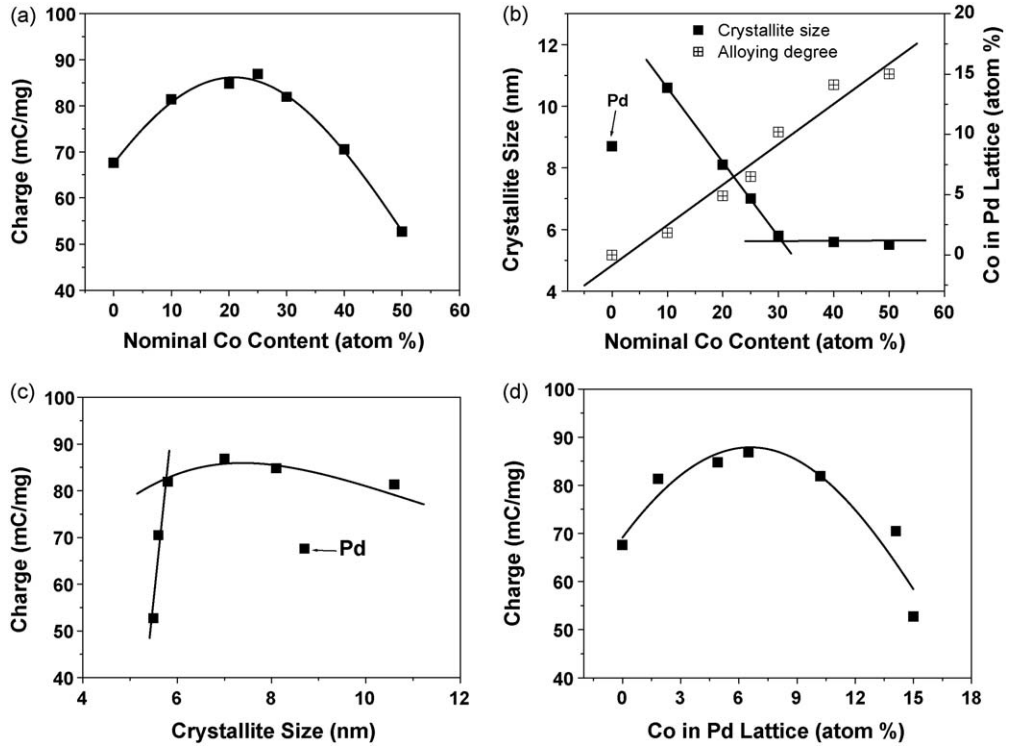

Fig. 8. Variations of the (a) catalytic activity with nominal Co content, (b) crystallite size and degree of alloying (Co content in the Pd lattice) with nominal Co content, (c) catalytic activity with crystallite size, and (d) catalytic activity with degree of alloying for the $Pd_{100-x}Co_x/C$ electrocatalysts after annealing at 350 °C.

g cm^{-3}. As the crystallite size increases with annealing temperature, the surface area decreases considerably (Table 1), which leads to a decrease in the number of active sites and catalytic activity.

Fig. 6 shows the XRD patterns of the $Pd_{100-x}Co_x/C$ samples with various nominal Co contents before and after annealing at 350 and 500 °C. While the reflections of the as-prepared Pd–Co samples do not shift in any noticeable way with Co content compared to that of

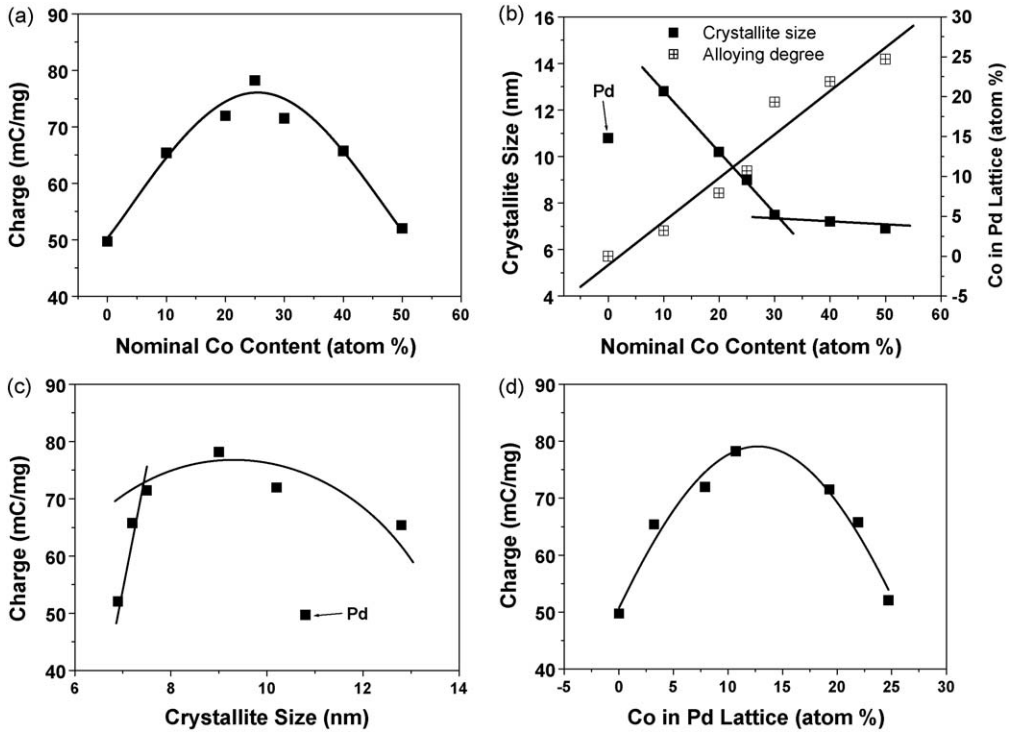

Fig. 9. Variations of the (a) catalytic activity with nominal Co content, (b) crystallite size and degree of alloying (Co content in the Pd lattice) with nominal Co content, (c) catalytic activity with crystallite size, and (d) catalytic activity with degree of alloying for the $Pd_{100-x}Co_x/C$ electrocatalysts after annealing at 500 °C.

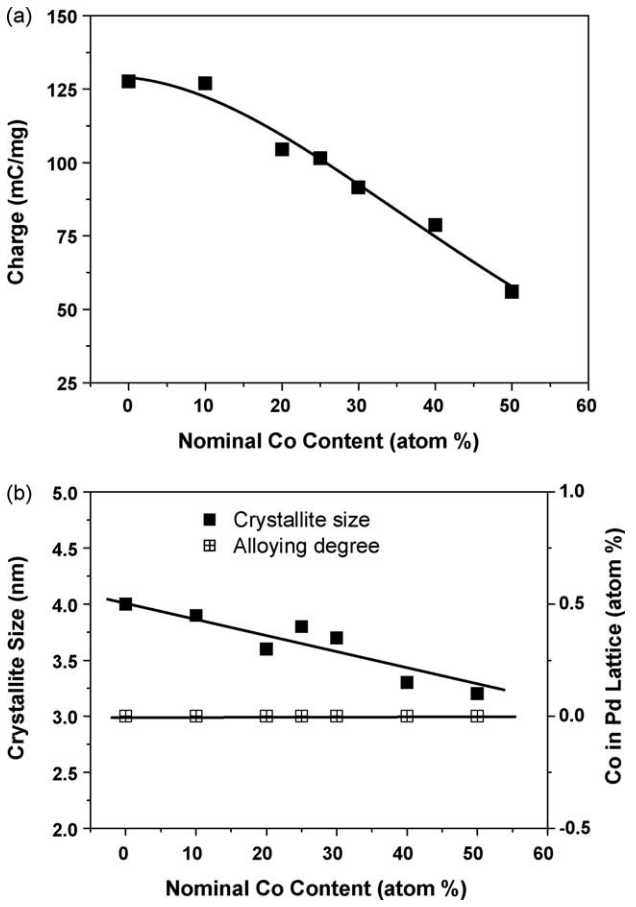

Fig. 10. Variations of the (a) catalytic activity with nominal Co content and (b) crystallite size and degree of alloying (Co content in the Pd lattice) with nominal Co content for the as-prepared $Pd_{100-x}Co_x$/C electrocatalysts.

Pd, they shift to higher angles on annealing with the shift increasing with both increasing Co content and annealing temperature. The shift is due to a substitution of smaller Co atoms for larger Pd atoms. The data suggest poor degree of alloying in the as-prepared samples and an increasing degree of alloying with Co content and annealing temperature.

Fig. 7 compares the CV scans recorded at the 15th cycle at room temperature of the $Pd_{100-x}Co_x$/C samples with various nominal Co contents before and after annealing at 350 and 500 °C. As pointed earlier, the electrocatalytic activities for ORR can be directly compared with the peak area values of the surface oxide reduction region in Fig. 7. As seen, for a given annealing temperature, the catalytic activity varies with the nominal Co content. In addition to the degree of alloying and crystallize size, the durability of the catalysts during the CV cycling can also influence the catalytic activity as the data presented are at the 15th cycle.

Fig. 8 shows the variations of the catalytic activity, crystallite size, and degree of alloying (actual amount of Co in the Pd lattice) with nominal Co content as well as the variations of the catalytic activity with crystallite size and degree of alloying for the samples annealed at 350 °C. Fig. 9 shows similar data for the samples annealed at 500 °C. The data in Figs. 8(b) and 9(b) reveal that the actual amount of Co in the Pd lattice (degree of alloying) is lower than the nominal Co content, and the degree of alloying for a given nominal Co content increases with increasing annealing temperature and for a given annealing temperature increases with increasing nominal Co content (Table 1). Also, the data in Figs. 8(b) and 9(b) reveal that the crystallite size for a given annealing temperature decreases rapidly with increasing nominal Co content up to 30 at% Co and then remains almost constant for nominal Co contents of 30–50 at%.

As discussed earlier, both the crystallite size and degree of alloying influence the catalytic activity and the catalytic activity of the $Pd_{100-x}Co_x$ electrocatalysts. Therefore, while the increase in the catalytic activity up to a nominal Co content of about

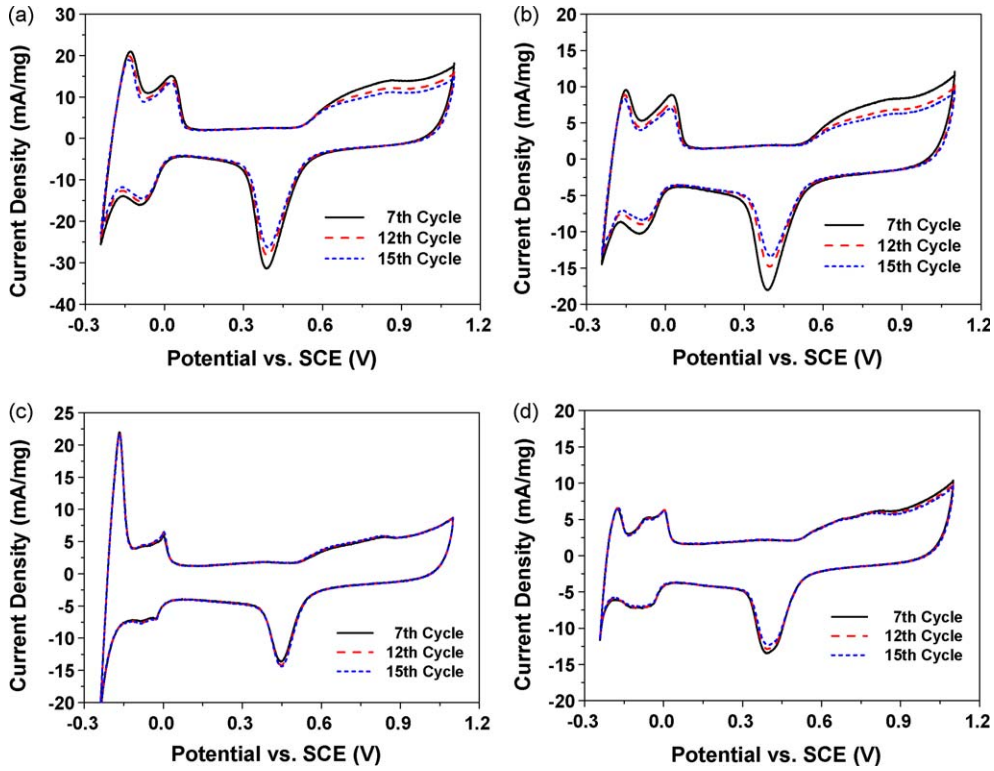

Fig. 11. Cyclic voltammograms of the Pd/C and $Pd_{50}Co_{50}$/C electrocatalysts in 0.5 M H_2SO_4 solution at a sweep rate of 20 mV s^{-1} at room temperature as a function of cycling: (a) as-prepared Pd/C, (b) as-prepared $Pd_{50}Co_{50}$/C, (c) Pd/C after annealing at 500 °C, and (d) $Pd_{50}Co_{50}$/C after annealing at 500 °C.

25 at% Co as seen in Figs. 8(a) and 9(a) can be considered to be due to both a decrease in crystallite size and an increase in degree of alloying as seen in Figs. 8(b) and 9(b), the decrease in catalytic activity in the 30–50 at% nominal Co content region is entirely due to the increasing degree of alloying as the crystallite size remains constant in this region (Figs. 8(b and c) and 9(b and c)). The latter demonstrates that increasing the degree of alloying (actual Co content in Pd lattice) beyond about 10 at% Co clearly causes a decrease in catalytic activity as seen in Figs. 8(d) and 9(d). One important observation is that Pd (without any Co) shows lower catalytic activity than the $Pd_{90}Co_{10}$ sample (with 10 at% nominal Co content) as seen in Figs. 8(a and c) and 9(a and c) despite a smaller crystallite size as seen in Figs. 8(b) and 9(b). This observation suggests that alloying Pd with a small amount of Co certainly helps to increase the catalytic activity.

The data also demonstrate that the increase in catalytic activity in the 0–30 at% nominal Co content is both due to a decrease in crystallite size and an increase in the degree of alloying. Thus, the combination of the two factors (crystallite size and degree of alloying) leads to an overall volcano relationship between catalytic activity and nominal Co content or actual Co content in the Pd lattice as seen in Figs. 8(a and d) and 9(a and d). The catalytic activity is maximized at a nominal Co content of about 25 at% nominal Co content or 7 and 11 at% actual Co content in the Pd lattice, respectively, for the 350 and 500 °C annealed samples. A core-shell structure for Pd-based alloys on annealing has been reported by some groups due to the migration of the noble metal Pd to the surface (phase segregation) [25,34–36]. In our study, the degree of alloying (Co content in the Pd lattice) increases with annealing temperature for all the Pd–Co alloy catalysts as seen in Fig. 5(c), suggesting changes in surface composition and potential after annealing.

However, a homogeneous alloy having both Pd and Co on the surface may be expected to give a favorable surface atomic structure for ORR due to the synergetic effect that may occur on combining Co having a high negative free energy for oxide formation that can help to cleave the O═O bond with Pd having a high standard reduction potential that can help to reduce the oxygen atoms to water [23,37]. In addition, as indicated by experimental data and density functional theory (DFT) calculations [29,30], presence of Co on the surface or under a Pd skin can modify the Pd–O bond energy to a balanced level to make the ORR more facile. Therefore, the migration of Co from the surface to the core on annealing could possibly decrease the catalytic activity with increasing degree of alloying.

Moreover, recent studies [38,39] have indicated that the Pd–Co subsurface structure is not stable in the presence of oxygen. The subsurface Co atoms have high potential to segregate to the surface with adsorbed oxygen. Thus, during the ORR experiment in presence of oxygen in our study, the surface structure and potential of the Pd–Co alloys could change (with Co segregating to the surface). Furthermore, the Co concentration on the surface could increase with increasing nominal Co content although the degree of alloying (Co content in the Pd lattice) increases with increasing nominal Co content in Pd–Co as seen in Figs. 8(b) and 9(b). Too much of Co on the surface layer could potentially decrease the catalytic activity due to the strong binding of oxygen. Thus, the catalytic activity decreases when the nominal Co content exceeds a critical value.

Fig. 10(a) shows the variation of the catalytic activity (or surface oxide reduction peak area at the 15th cycle) with nominal Co content for the as-prepared $Pd_{100-x}Co_x$/C samples. In contrast to the volcano type relationship between the catalytic activity and the nominal Co content in Figs. 8 and 9 for the annealed samples, the activity of the as-prepared samples exhibit a monotonous decrease with increasing nominal Co content from 0 to 50 at% Co. Fig. 10(b) shows the variations of crystallite size and degree of alloying (actual Co content in the Pd lattice) with nominal Co content for the $Pd_{100-x}Co_x$/C-Ap samples. As seen, the degree of alloying determined from the lattice parameter values is almost zero for the entire nominal Co content (0–50 at% Co), while the crystallite size decreases only slightly with increasing nominal Co content. Therefore, the effect of both the degree of alloying and crystallite size on the catalytic activity can be considered to be negligible. The monotonous decrease in activity with increasing nominal Co content is essentially due to the decreasing Pd wt.% in the catalyst as Co by itself is inactive and chemically more unstable.

In order to assess the durability of the $Pd_{100-x}Co_x$/C samples, multiple CV scans were carried out. Fig. 11 displays the CV scans of the 7th, 12th, and 15th cycles for the as-prepared and 500 °C annealed Pd/C and $Pd_{50}Co_{50}$/C samples. While both the as-prepared samples exhibit a decline in activity on cycling, the 500 °C samples show much better durability. Moreover, the activity of the as-prepared samples decreases faster on going from Pd/C to $Pd_{50}Co_{50}$/C, possibly due the easier dissolution of Co.

Fig. 12 shows the variation of catalyst durability with nominal Co content for the as-prepared and 500 °C annealed $Pd_{100-x}Co_x$/C samples. The % durability values were obtained as the percentage ratio of the surface oxide reduction peak area in the 15th cycle to that in the 7th cycle. As seen, the durability is lower and decreases

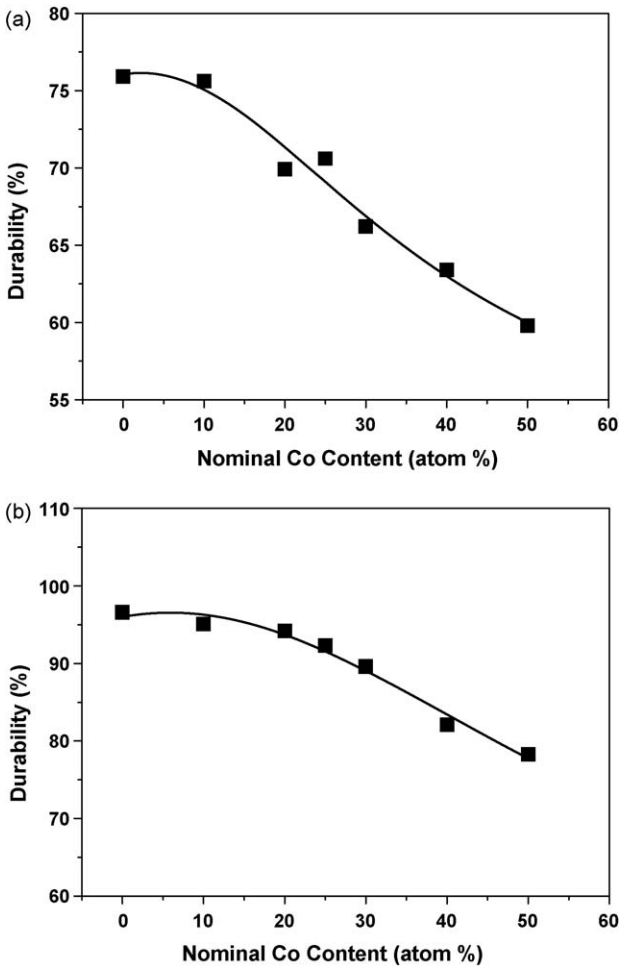

Fig. 12. Variations of the durability of the a $Pd_{100-x}Co_x$/C electrocatalysts with nominal Co content: (a) as-prepared samples and (b) after annealing at 500 °C.

monotonously with increasing nominal Co content from 0 to 50 at% Co for the as-prepared samples. The decreasing durability of the as-prepared samples on cycling in the acidic environment could be due to both the leaching out of the poorly alloyed Co and the smaller particle size (high surface area). Recent theoretical calculations have indicated that Co in Pd–Co alloys is likely to be stripped out at lower potentials in acid solutions [40], so higher Co contents in the as-prepared samples could lead to a faster decline in activity. However, the as-prepared Pd/C sample (with no Co) also exhibit a decrease in activity on cycling, which could be attributed mainly due to the smaller crystallite size. Therefore, the catalytic activity of the as-prepared $Pd_{100-x}Co_x/C$ samples with varying Co content is largely affected by their durability, which masks the influence of crystallite size and the degree of alloying. Interestingly, the samples annealed at 500 °C exhibit much improved durability in acid solutions due to an increasing degree of alloying. Thus, a mild annealing at moderate temperatures may be desirable to clean the electrocatalyst surface to realize high catalytic activity and to enhance the degree of alloying with Co to realize acceptable durability.

4. Conclusions

With a systematic investigation of the $Pd_{100-x}Co_x/C$ ($0 \leq x \leq 50$) electrocatalysts, a volcano type dependence of the catalytic activity for ORR on nominal Co content is found for the samples annealed at 350 and 500 °C, while a monotonously decrease in activity is found for the as-prepared samples. The volcano type dependence for the former with the maximum activity around 25 at% nominal Co content or around 10 at% Co in the Pd lattice (degree of alloying) is due to the influence of both the degree of alloying and crystallite size on the activity, while the monotonous dependence for the latter is due to the poor durability. While both a decrease in the crystallite size and an increase in the degree of alloying contribute to the increase in catalytic activity with increasing nominal Co content up to 30 at% Co for the annealed samples, the increasing degree of alloying in the region 30–50 at% Co causes a decrease in activity as the crystallite size remains constant in this region. The durability of the $Pd_{100-x}Co_x/C$ electrocatalysts increases with increasing annealing temperature due to an increasing degree of alloying of Pd with Co and an increase in crystallite size. Thus, a mild annealing of the alloys at moderate temperatures (~350 °C) may be desirable to clean the surface and maximize the catalytic activity and durability despite a moderate increase in crystallite size. The study demonstrates that an in-depth understanding of the various factors that influence the catalytic activity of the $Pd_{100-x}Co_x$ nanoalloys can help to design and develop high performance low cost alloy catalysts for fuel cells.

Acknowledgments

Financial support by the National Science Foundation grant CBET-0651929 and the MURI grant no. N00014-07-1-0758 is gratefully acknowledged.

References

[1] H.A. Gasteiger, S. Kocha, B. Sompalli, F.T. Wagner, Appl. Catal. B 56 (2005) 9–35.
[2] V.R. Stamenkovic, B. Fowler, B.S. Mun, G. Wang, P.N. Ross, C.A. Lucas, N.M. Marković, Science 315 (2007) 493–497.
[3] N. Tian, Z. Zhou, S. Sun, Y. Ding, Z. Wang, Science 316 (2007) 732–735.
[4] J.G. Chen, Chem. Rev. 96 (1996) 1477–1498.
[5] J.M. Zen, C.B. Wang, J. Electrochem. Soc. 141 (1994) L51–L52.
[6] N. Mano, J.L. Fernandez, Y. Kim, W. Shin, A.J. Bard, A. Heller, J. Am. Chem. Soc. 125 (2003) 15290–15291.
[7] N. Mano, H.H. Kim, Y. Zhang, A. Heller, J. Am. Chem. Soc. 124 (2002) 6480–6486.
[8] S. Ye, A.K. Vijh, Electrochem. Commun. 27 (2003) 272–275.
[9] R. Pattabhiraman, Appl. Catal. A 153 (1997) 9–20.
[10] O. Savadago, K. Lee, K. Oishi, S. Mitsushima, N. Kamiya, K.I. Ota, Electrochem. Commun. 6 (2004) 105–109.
[11] M. Watanabe, K. Tsurumi, T. Mizukami, T. Nakamura, P. Stonehart, J. Electrochem. Soc. 141 (1994) 2659–2668.
[12] L. Xiong, A. Manthiram, J. Mater. Chem. 14 (2004) 1454–1460.
[13] L. Xiong, A. Manthiram, J. Electrochem. Soc. 152 (2005) A697–A703.
[14] V.R. Stamenkovic, T.J. Schmidt, P.N. Ross, N.M. Markovic, J. Phys. Chem. B 106 (2002) 11970–11979.
[15] V. Raghuveer, A. Manthiram, Electrochem. Solid-State Lett. 7 (2004) A336–A339.
[16] T. Toda, H. Igarashi, H. Uchida, M. Watanabe, J. Electrochem. Soc. 146 (1999) 3750–3756.
[17] M.C.R. Martinez, D.C. Amoros, A.L. Salano, C.S. Martinez, H. Yamashita, M. Anpo, Carbon 33 (1995) 3–13.
[18] S. Mukerjee, S. Srinivasan, M. Soriaga, J. Electrochem. Soc. 142 (1995) 1409–1422.
[19] S.H. Joo, S.J. Choi, M. OH, J. Kwak, Z. Liu, O. Terasaki, R. Ryoo, Nature 412 (2001) 169–172.
[20] T. Toda, H. Igarashi, M. Watanabe, J. Electroanal. Chem. 460 (1999) 258–262.
[21] J.L. Fernandez, V. Raghuveer, A. Manthiram, A.J. Bard, J. Am. Chem. Soc. 127 (2005) 13100–13101.
[22] V. Raghuveer, A. Manthiram, A.J. Bard, J. Phys. Chem. 109 (2005) 22909–22912.
[23] V. Raghuveer, P.J. Ferreira, A. Manthiram, Electrochem. Commun. 8 (2006) 807–814.
[24] H. Liu, A. Manthiram, Electrochem. Commun. 10 (2008) 740–744.
[25] M.H. Shao, K. Sasaki, R.R. Adzic, J. Am. Chem. Soc. 128 (2006) 3526–3527.
[26] M.H. Shao, P. Liu, J. Zhang, R.R. Adzic, J. Phys. Chem. B 111 (2007) 6772–6775.
[27] K. Lee, O. Savadogo, A. Ishihara, S. Mitsushimas, N. Kamiya, K.I. Ota, J. Electrochem. Soc. 153 (2006) A20–A24.
[28] Y. Suo, L. Zhuang, J. Lu, Angew. Chem. Int. Ed. 46 (2007) 2862–2864.
[29] T. Bligaard, J.K. Nørskov, Electrochim. Acta 52 (2007) 5512–5516.
[30] J.R. Kitchin, J.K. Nørskov, M.A. Barteau, J.G. Chen, Phys. Rev. Lett. 93 (2004) 156801-1–156801-4.
[31] R. Narayanan, M.A. Ei-Sayed, Nano Lett. 4 (2004) 1343–1348.
[32] M. Peuckert, T. Yoneda, R.A. Dalla, M. Boudart, J. Electrochem. Soc. 133 (1986) 944–947.
[33] N. Giordano, E. Passalacqua, L. Pino, A.S. Arico, V. Antonucci, M. Vivaldi, K. Kinoshita, Electrochim. Acta 36 (1991) 1979–1984.
[34] M.H. Shao, T. Huang, P. Liu, J. Zhang, K. Sasaki, M.B. Vukmirovic, R.R. Adzic, Langmuir 22 (2006) 10409–10415.
[35] A.V. Ruban, H.L. Skriver, J.K. Nørskov, Phys. Rev. B 59 (1999) 15990–16000.
[36] J.L. Rousset, J.C. Bertolini, P. Miegge, Phys. Rev. B 53 (1996) 4947–4957.
[37] J.L. Fernandez, D. Walsh, A.J. Bard, J. Am. Chem. Soc. 127 (2005) 357–365.
[38] C.A. Menning, J.G. Chen, J. Chem. Phys. 128 (2008) 164703-1–164703-9.
[39] Y. Xu, A.V. Ruban, M. Mavrikakis, J. Am. Chem. Soc. 126 (2004) 4717–4725.
[40] J. Greeley, J.K. Nørskov, Electrochim. Acta 52 (2007) 5829–5836.